



Directed nucleation and growth by balancing local supersaturation and substrate/nucleus lattice mismatch

Citation

Li, L., A. J. Fijneman, J. A. Kaandorp, J. Aizenberg, and W. L. Noorduin. 2018. "Directed Nucleation and Growth by Balancing Local Supersaturation and Substrate/nucleus Lattice Mismatch." *Proceedings of the National Academy of Sciences* 115 (14) (March 19): 3575–3580. doi:10.1073/pnas.1712911115.

Published Version

doi:10.1073/pnas.1712911115

Permanent link

<http://nrs.harvard.edu/urn-3:HUL.InstRepos:37235083>

Terms of Use

This article was downloaded from Harvard University's DASH repository, and is made available under the terms and conditions applicable to Open Access Policy Articles, as set forth at <http://nrs.harvard.edu/urn-3:HUL.InstRepos:dash.current.terms-of-use#OAP>

Share Your Story

The Harvard community has made this article openly available.
Please share how this access benefits you. [Submit a story](#).

[Accessibility](#)

Directed nucleation and growth by balancing local supersaturation and substrate/nucleus lattice mismatch

L. Li,^{1,2,3} A. J. Fijneman,^{1,4} J. A. Kaandorp,⁵ J. Aizenberg,^{1,2,6,7} W. L. Noorduin,^{1,8}

¹John A. Paulson School of Engineering and Applied Sciences, Harvard University, Cambridge, MA 02138, USA

²Wyss Institute for Biologically Inspired Engineering, Harvard University, Boston, MA 02115, USA

³Department of Mechanical Engineering, Virginia Polytechnic Institute and State University, Blacksburg, VA 24060, USA

⁴Department of Chemical Engineering and Chemistry, Eindhoven University of Technology, 5612 AZ Eindhoven, The Netherlands

⁵Computational Science Lab, Faculty of Science, University of Amsterdam, 1098 XH Amsterdam, The Netherlands

⁶Kavli Institute for Bionano Science and Technology, Harvard University, Cambridge, MA 02138, USA

⁷Department of Chemistry and Chemical Biology, Harvard University, Cambridge, MA 02138, USA

⁸AMOLF, 1098 XG Amsterdam, The Netherlands.

Controlling nucleation and growth is crucial in biological and artificial mineralization and self-assembly processes. The nucleation barrier is determined by the interfaces and local supersaturation. Although chemically tailored substrates and lattice mismatches are routinely used to modify various forms of energy contributions as resulted from the substrate/nucleus interface and thereby steer controlled heterogeneous nucleation, strategies to combine this with control over local supersaturations have remained virtually unexplored. Here we demonstrate simultaneous control over both parameters to direct the positioning and growth direction of mineralizing compounds on preselected polymorphic substrates. We exploit the polymorphic nature of calcium carbonate (CaCO_3) to locally manipulate the carbonate concentration and lattice mismatch between the nucleus and substrate, such that barium carbonate (BaCO_3) and strontium carbonate (SrCO_3) nucleate only on specific CaCO_3 polymorphs. Based on this approach we position different materials and shapes on predetermined CaCO_3 polymorphs in sequential steps, and guide the growth direction using locally created supersaturations. These results shed light on nature's remarkable mineralization capabilities and outline new fabrication strategies for advanced materials, such as ceramics, photonic structures and semiconductors.

Significance

The energy barrier for a classical heterogeneous crystal nucleation can be controlled by the energy contributions from the substrate/nucleus interface and local supersaturation. Exerting control over crystal growth thus requires modifying either one of these terms. We here introduce a strategy to modulate the contributions of *both* parameters simultaneously using substrates containing different crystal structures of calcium carbonate. Based on a theoretical analysis, we program both the positioning and growth direction of carbonate salts on preselected polymorphs. These findings may hold relevance for understanding, mimicking and ultimately expanding upon nature's mineralization strategies and for developing functional microscale materials.

\body

Spurred by the recent advancement in techniques such as microfabrication and electron microscopy, there has been tremendous advancement in understanding and controlling both

biological and artificial mineralization processes (1-4). Unlike homogeneous nucleation, heterogeneous nucleation allows for an effective strategy to control the local nucleation energy barrier by modifying the chemical and structural characteristics between the nascent nucleus and substrates (5-12). Alternatively, a local increase of the supersaturation can onset nucleation (13-15) – an approach broadly utilized by natural systems through ion channels that deliver crystallizing components to the specific site where nucleation should occur, – but this approach has hardly been explored in artificial systems. Only recently, such local supersaturations were created using an ion binding biomimetic matrix (4). However, little or no work has been done to develop principles that allow for simultaneous control over the local supersaturation and interfacial free energy for directing the nucleation position, let alone the growth (15).

While virtually all previous studies have been aimed at avoiding polymorphism (16), we here use the ability of compounds to organize in different crystal forms to rationally control local supersaturations in the vicinities of different polymorphs and subtle variations in the lattice mismatch between the substrate and the nucleus. An ideal model system to test this strategy is the crystallization of BaCO₃ selectively on top of different polymorphs of CaCO₃. CaCO₃ is the most abundant biomineral and can be found in three anhydrous polymorphs that all occur in living organisms (17-23). At room temperature calcite is the most stable polymorph, followed by aragonite and finally vaterite as the least stable structure. To demonstrate the ability to tune the positioning of BaCO₃ on top of these polymorphs and its growth direction, we analyze and exploit local variations of supersaturations induced by the difference in the dissolution rate of CaCO₃ polymorphs. Additionally, the crystal structures of calcite, aragonite, and vaterite are different from each other, and only aragonite resembles that of BaCO₃ (23). This variation in crystal structures allows for direct evaluation of the effects of the lattice mismatch on templated nucleation of BaCO₃ on selected CaCO₃ polymorphs modulated by the local supersaturation gradients.

Results and Discussions

To understand the unique interplay between the interfacial free energy that arises from the lattice mismatch and supersaturation in this system, we analyze a solution containing Ba²⁺ ions in which an influx of CO₃²⁻ causes the templated nucleation of BaCO₃ on a CaCO₃ substrate with crystal structure x (Fig. 1). According to classical nucleation theory (13-15), the energy barrier to form a critical nucleus, Δg_n , can be described as a function of the local supersaturation σ and the interfacial free energy α according to

$$\Delta g_n \propto \frac{\alpha_x^3}{\sigma_x^2} . \quad (1)$$

The lattice mismatch between the BaCO₃ nucleus and the underlying substrate directly contributes to the interfacial energy penalties, which include an energy contribution due to the difference in chemical bonding, and a strain energy contribution from the interface and the nucleate volume that arises from the incoherent ordering at the interface. Although analytical expressions of each energy contribution are hard to achieve due to the complexity of the system, both energy contributions should decrease as the substrate/nucleus interface becomes more crystallographically aligned and coherent.

The energy gain resulting from the chemical potential energy is directly related to the supersaturation of BaCO₃. In case the substrate has a higher solubility than the nucleating compound, and the rate of dissolution of the substrate is higher than the rate of growth of the nucleating crystal (Fig. 1), the supersaturation in BaCO₃ can be expressed as:

$$\sigma = \ln \left(\frac{k_{BaCO_3} [Ba^{2+}] [CO_3^{2-}]_{bulk}}{k_{BaCO_3} [Ba^{2+}] - k_x + k_x' [Ca^{2+}]_s} \right) \quad (2)$$

with k_{BaCO_3} the crystallization rate constant of $BaCO_3$, $[CO_3^{2-}]_{bulk}$ the concentration of carbonate in the bulk solution, $[Ca^{2+}]_s$ the Ca^{2+} concentration close to the surface of the $CaCO_3$ crystal, k_x the dissolution rate constant of $CaCO_3$ for a specific polymorph x , and $k_x' = k_{CaCO_3,x} / K_{sp,CaCO_3,x}$ where $K_{sp,CaCO_3,x}$ is the solubility product of a specific polymorph x of $CaCO_3$ (see SI, 24-27). We assume $k_{vaterite} > k_{aragonite} > k_{calcite}$ and $K_{sp,vaterite} > K_{sp,aragonite} > K_{sp,calcite}$, which implies that both the dissolution rate and solubility of vaterite is higher than those for aragonite and calcite. In case of ample availability of Ba^{2+} , the free energy barrier Δg_n for nucleation on a specific polymorph of $CaCO_3$ is controlled by the interplay of: (a) the concentration of carbonate from the bulk solution, (b) the polymorph-dependent lattice mismatch of the $CaCO_3$ substrate, and (c) the substrate solubility equilibrium. We therefore expect that the choice of the positioning of the nucleation can be tuned by the subtle changes in relative contributions of these parameters. Below we consider various scenarios where the impact of these parameters is analyzed and exploited to direct the nucleation and growth of $BaCO_3$.

To evaluate the effects of lattice mismatch in the carbonate system studied here, we characterized the crystallographic relationships of $BaCO_3$ grown on top of calcite, aragonite and vaterite as substrate crystals. The overgrown $BaCO_3$ crystals can be easily differentiated from the underlying $CaCO_3$ crystals in backscatter electron microscopy due to their electron density difference (Fig. 2A, i, ii). Through focused ion beam (FIB) milling, electron-transparent transmission electron microscopy (TEM) samples were prepared at the interfaces of nucleus and substrates, from which the morphological and crystallographic characteristics were evaluated (Fig. 2A, iii-v). $BaCO_3$ exhibit well alignment with calcite and aragonite by sharing the same c -axes, while vaterite showed no crystallographic alignment (Fig. 2A; see Supplementary Information). This lack of orientation matching thus indicates a higher interfacial free energy for nucleation on vaterite as compared to calcite and aragonite. A qualitative estimation of the lattice mismatch shows that $BaCO_3$ has a slightly smaller lattice mismatch in both a and b directions on calcite as the substrate in comparison to aragonite as the substrate (SI, section 8) (12). Therefore, when all three polymorphs are present as crystallization substrates, $BaCO_3$ will selectively first nucleate on calcite, followed by aragonite, but not on vaterite for the same supersaturation levels. On the other hand, substrate solubility should favor the nucleation of $BaCO_3$ on vaterite over crystallization on aragonite, and least on calcite, due to significant local supersaturation occurring on the surfaces of the dissolving vaterite at low values of bulk carbonate content. The relative contributions of these two factors can be easily tuned by varying $[CO_3^{2-}]_{bulk}$, according to Eqs. 1-2. For high values of the $[CO_3^{2-}]_{bulk}$ the lattice mismatch is expected to dominate the crystallization position, whereas for low values of $[CO_3^{2-}]_{bulk}$ the solubility equilibrium of the substrate will increase the supersaturation in the vicinity of the least stable polymorphs.

These differences in lattice mismatches, in combination with external control over the local supersaturation allow us to selectively nucleate $BaCO_3$ on a predetermined polymorph of $CaCO_3$. To probe the influence of $[CO_3^{2-}]_{bulk}$, we developed a method to fabricate mixed polymorphic substrates containing all three polymorphs of $CaCO_3$ (typically, calcite $79 \pm 8\%$, aragonite $14 \pm 5\%$ and vaterite $7 \pm 3\%$) by crystallizing $CaCO_3$ on an aluminum plate (see SI for details and setup). We vertically positioned the substrate containing all three $CaCO_3$ polymorphs in the reaction solution. As carbonate from the air entered the solution from the top, a $[CO_3^{2-}]$ gradient was created along the substrate, thus allowing for a continuous combinatorial screening of the influence of the $[CO_3^{2-}]_{bulk}$ on the overgrowth of the $CaCO_3$ polymorphs. To quantify the results,

we manually counted each polymorph as a function of the depth (Fig. 2B). We define the polymorph overgrowth ratio $R_{Ba,x}$ for a specific CaCO_3 polymorph x as $R_{Ba,x} = (n_{Ba,x}/n_x)/\sum_x(n_{Ba,x}/n_x)$, with n_x denoting the total number of CaCO_3 crystals of a specific polymorph x ; $n_{Ba,x}$ the number of CaCO_3 crystals of this polymorph that have been overgrown with BaCO_3 , and the sum in the nominator running over all possible polymorphs (Fig. 2C). Additionally, we compute the cumulative distribution function (CDF) for each overgrown polymorph as a function of the depth in the solution (Fig. 2D).

Close to the meniscus (0.0-0.5 mm), the $[\text{CO}_3^{2-}]_{bulk}$ is the highest, which minimizes the effect of the local carbonate supersaturation due to polymorph dissolution. The lattice mismatch thus dominates the nucleation position, and BaCO_3 only nucleates on calcite and aragonite, with no nucleation on vaterite, which is expected as the lack of crystallographic alignment on vaterite results in a disadvantageous lattice mismatch. Deeper in the solution (0.5-2.0 mm), the lower $[\text{CO}_3^{2-}]_{bulk}$ decreases the local supersaturation around the calcite and aragonite crystals, and fewer of them become overgrown with BaCO_3 . The lower $[\text{CO}_3^{2-}]_{bulk}$ also increases the dissolution of the least stable polymorph following Eq. 2, thus locally increasing the supersaturation around the vaterite crystals. Since the solubility of BaCO_3 is approximately tenfold lower than that of CaCO_3 polymorphs ($K_{sp,BaCO_3} \ll K_{sp,CaCO_3,x}$), the increase in CO_3^{2-} concentration around the dissolving vaterite crystals onsets the nucleation of BaCO_3 . Below 2.0 mm $[\text{CO}_3^{2-}]_{bulk}$ the supersaturation is too low for nucleation on either calcite or aragonite crystals even though the lattice mismatch is favorable for these substrates. The stability-dependent dissolution completely dominates the nucleation and all vaterite crystals become overgrown. Dissolving vaterite crystals even increases the local CO_3^{2-} concentration to such an extent that crystallization of BaCO_3 may occur on an accidental calcite and aragonite crystal grown in close proximity to vaterite (Fig. SI 2B). It should be noted that a similar trend is found for the overgrowth of CaCO_3 polymorphs with SrCO_3 instead of BaCO_3 (Fig. SI 3), demonstrating that these principles can readily be extended to other systems. Furthermore, precise control over the spatial location and polymorphism of the CaCO_3 substrates may be gained using patterned self-assembled monolayers (11).

In order to create more complex shapes beyond the simple morphology of BaCO_3 crystals, we introduce silica to the reaction. The resulting $\text{BaCO}_3/\text{SiO}_2$ structures can straightforwardly be sculpted in a rich pallet of microshapes such as vases, spirals and corals by externally modulating the reaction conditions, such as pH and temperature (28-31). The formation of these various shapes and their orientation is highly sensitive to and nearly fully determined by the concentrations of the reacting species in the vicinity of the developing structures, and can therefore act as an ideal model system to test the sensitivity of the nucleation events described above. Recently, we have also shown that precise control of the shape could lead to functional shapes such as those that can be used in photonics (31). In particular, by integrating a fluorescent dye as a light source in the nucleating barium carbonate seed crystal, effective waveguiding and beamsplitting through the rationally designed microarchitectures were achieved. While in this previous work no control over the position of these structures was obtained, the present study can introduce the ability to precisely control the location of the nucleation of these microstructures. Moreover, we anticipated that akin to chemotaxis, the creation of the local gradient in supersaturation induced by specific polymorphs of CaCO_3 placed in the immediate vicinity of the nucleating microstructures may be used to steer the growth of these structures in predetermined directions.

The precipitation of these $\text{BaCO}_3/\text{SiO}_2$ structures starts with the formation of a BaCO_3 crystal, which to a good approximation is not affected by the SiO_2 . Hence we can assign the nucleation

position in a manner analogous to how we directed the nucleation of BaCO₃ (Fig. 3A,B). Indeed, we find the same trend: preferred nucleation on calcite and aragonite at low immersion depths, whereas nucleation on vaterite only occurs deeper in the solution. Importantly, the ratio between the overgrown aragonite and calcite crystals in the top of the substrate gradually increases, with aragonite crystals being selectively overgrown at 0.75-1.5 mm (Fig. 3B), likely due to the growing contribution of the increase in local supersaturation from the dissolving calcium carbonate in the BaCO₃/aragonite system over the BaCO₃/calcite, as the bulk concentration in CO₂ goes down. It should be noted that the silica hampers the nucleation of BaCO₃. As a result, we observe a zone (2.0-5.0 mm) where the local supersaturation is insufficient to grow BaCO₃/SiO₂ structures and only below 5.0 mm is the local supersaturation sufficiently high to induce nucleation on vaterite. More complex shapes can be grown by rationally adjusting the reaction conditions, as exemplified by the SrCO₃/SiO₂ stems in Fig. 3C that were opened into vases using a CO₂ pulse and subsequently decorated with serrated edges using temperature modulations.

The ability to control nucleation on preselected polymorphs can also be used for positioning different materials on assigned polymorphs in sequential steps. We demonstrated this by first growing CaCO₃ spirals in the presence of polyaspartic acid (PAA) (32, 33). As these spirals are composed of vaterite nanocrystals, they selectively form on vaterite in the presence of all three polymorphs independent of the depth (Fig. 3D). With both the calcite and aragonite crystals still available, we subsequently positioned BaCO₃/SiO₂ spirals on the aragonite crystals while leaving the calcite crystals bare (Fig. 3E) at a depth of 1.5 mm.

Due the sensitivity of the BaCO₃/SiO₂ coprecipitation to local gradients, one can further define the growth direction of these sophisticated structures e.g. spirals, towards locally positioned carbonate sources. We ascertained this by growing BaCO₃/SiO₂ spirals on a substrate containing the mixture of CaCO₃ polymorphs at a depth of ca. 1.5 mm. According to Fig. 3B, at this depth the nucleation of BaCO₃ preferentially occurs on aragonite whereas neighboring vaterite gradually dissolves, thus causing a local increase in [CO₃²⁻] that could attract the growth front of the BaCO₃/SiO₂ structure and induce its directional chemotaxis. Indeed, we observed that BaCO₃/SiO₂ spirals first formed on aragonite, and subsequently grew only towards nearby dissolving vaterite, while not being influenced by neighboring calcite (Fig. 4). It should be noted that in the absence of silica, we also found that dissolving vaterite crystals could induce sufficient carbonate concentrations to induce nucleation on nearby calcite and vaterite crystals (Fig. SI 2B). Selectively lowering the relative energy barrier for nucleation on one polymorph and creating a nearby local supersaturation by dissolving another polymorph thus provides simultaneous control over both the nucleation on preselected polymorphs and growth direction.

Summary and Conclusions

In conclusion, we have introduced a strategy to control the polymorph-specific positioning of mineralizing compounds and their directional growth using substrates with polymorphic mixtures as crystallization templates. The power of our approach is that merely the influx of carbonate allows us to manipulate the local concentrations of the crystallizing ions within a landscape of different interfacial energies. Therefore, by simultaneously controlling the concentration of carbonate from the bulk solution, the polymorph-dependent interfacial energy contribution from the lattice mismatch, and the substrate solubility, we are able to elicit unusual mineralization pathways unachievable by separate control over these individual parameters. In contrast with commonly used nucleation techniques that are based on lowering of the interfacial free energy only, we can therefore also nucleate selectively on substrates that have an unfavorable crystallographic alignment. Additionally, we can sequentially position different materials on assigned polymorphs and steer the growth of these structures in directions predetermined by the

location of neighboring dissolving species. These concepts can perfect our ability to control nucleation and growth of nanostructured materials and may elucidate mechanisms that regulate nano- and microscale phenomena in biomineralization processes.

Methods

Crystallization of CaCO₃ polymorphic substrates. For the crystallization of mixed polymorphs of CaCO₃, 0.032 g of CaCl₂ was dissolved in 15 mL water in a 50 or 100 mL beaker. An aluminum slide (ca. 15x15x1 mm), or aluminum-coated microscope glass slide, was vertically positioned in the solution and the beaker was placed in a closed desiccator with freshly ground (NH₄)₂CO₃ following the method developed by Addadi *et al.* (6). After ca. 30-45 min, the slide was removed from the solution, washed twice with water and then washed with acetone and dried on the air. For details see SI Appendix, section 1.

Overgrowth of a CaCO₃ polymorph mixture with BaCO₃. In a 50 or 100 mL beaker, we dissolved 0.074 g BaCl₂ in 15 mL water and adjusted the pH to 11.9 using NaOH. A previously prepared slide with a mixture of calcite, aragonite and vaterite (see above) was positioned at a 90° angle in the solution such that a half of the previously overgrown area (shown schematically as a green line in Fig. SI2A, left) was submerged. A petri dish was loosely placed on the beaker allowing for the CO₂ from the air to enter the beaker. After ca. 30-45 min, the slide was removed from the solution, washed twice with water and then washed with acetone and subsequently dried. Optical microscopy and SEM were used to analyze the slide and quantify the crystallization of the BaCO₃ on the CaCO₃ mixture. For details see SI Appendix section 2 and for overgrowth with SrCO₃ SI Appendix, section 3.

Overgrowth of a CaCO₃ polymorph mixture with BaCO₃/SiO₂ microstructures. In a 50 or 100 mL beaker, we dissolved 0.074 g of BaCl₂ and 0.016 g of Na₂SiO₃ in 15 mL water. To grow stem, vase and coral shaped structures, the pH was adjusted to pH 11.9 whereas for growth helices the pH was adjusted to 11.1 (30). A previously prepared slide with a mixture of calcite, aragonite and vaterite (see above) was positioned at 90° in the solution such that half of the previously overgrown area was submerged in the solution. A petri dish was loosely placed on the beaker such that CO₂ from the air could enter the beaker. After ca. 45 – 120 min, the slide was removed from the solution, washed twice with water and then washed with acetone and dried in the air. Optical microscopy and SEM were used to analyze the results.

Overgrowth of a CaCO₃ polymorph mixture with CaCO₃/PAA microstructures. In a 50 or 100 mL beaker, we dissolved 0.032 g of CaCl₂ and between 60 and 120 µg/mL poly (α ,L-aspartate) (Sigma Aldrich) in 15 mL water. A previously prepared slide with a mixture of calcite, aragonite and vaterite (see above) was position under positioned at 90° in the solution such that half of the previously overgrown area was submerged. The beaker was placed in a closed desiccator with freshly ground (NH₄)₂CO₃ and placed in an oven at 45 °C. After ca. 45 – 120 min, the slide was removed from the solution, washed twice with water and then washed with acetone and dried in the air. Optical microscopy, Raman microscopy and SEM were used to analyze the slide.

FIB/TEM procedure. Samples were coated with Au (~5 nm) to reduce charging effects prior to focused ion beam (FIB) milling with a Helios Nanolab 660 Dual Beam electron microscope (FEI, OR). Typical TEM sample preparation procedure was as follows: 1) a platinum protective layer (~0.5 µm) was first laid down on top of the desired structure; 2) another platinum protective layer (~1.5 µm) was further deposited on top of the rectangular region where the TEM slab was to be milled out; 3) two sides of the coated structure, were milled away by FIB, leaving the slab of specimen (thickness: ~1.5 µm); 4) the slab was then cut through by FIB and transferred to a

copper TEM grid by an Omniprobe and welded securely with platinum deposition; 5) the lift-out lamellar of specimen was sequentially thinned by FIB at 30, 16, 5, and 2 kV ion beam voltages. Final cleaning at 2 kV and 28 pA is important to obtain a clean surface and minimize damage. TEM imaging was carried out using a JEOL 2011 operated at 120 kV. For detailed section 6-8 in the SI Appendix for detailed figures, analysis of the crystal structure and calculation of the crystallographic mismatch.

Acknowledgements

Dr. Liesbeth Janssen and Prof Pieter Rein ter Wolde are kindly acknowledged for help with the manuscript. This research was supported by the NSF DMREF under award 15-33985 and the Harvard MRSEC under award DMR 14-20570. WLN thanks the Netherlands Organization for Scientific Research (NWO) for financial support from a VENI grant. LL thanks the Department of Mechanical Engineering at Virginia Tech for support. Electron microscopy and focused ion beam milling was performed at the Center for Nanoscale Systems at Harvard University, supported by the NSF under award ECS-0335765, and at the Amsterdam nanoCenter, which was financially supported by NWO.

References

1. De Yoreo, J. J. *et al.* (2015) Crystallization by particle attachment in synthetic, biogenic, and geologic environments. *Science* **349**, 498.
2. Wegst, U. G. K., Bai, H., Saiz, E., Tomsia, A. P., Ritchie, R. O. (2014) Bioinspired structural materials. *Nature Mat.* **14**, 23-36.
3. Nielsen, M. H., Aloni, S., De Yoreo, J. J. (2014) In situ TEM imaging of CaCO₃ nucleation reveals coexistence of direct and indirect pathways. *Science* **345**, 1158-1162.
4. Smeets, P. J. M., Cho, K. R., Kempen, R. G. E., Sommerdijk, N. A. J. M., De Yoreo, J. J. (2015) Calcium carbonate nucleation driven by ion binding in a biomimetic matrix revealed by in situ electron microscopy. *Nature Mat.* **14**, 394-399.
5. Addadi, L. & Weiner, S. (1985) Interactions between acidic proteins and crystals: stereochemical requirements in biomineralization. *Proc. Natl. Acad. Sci.* **82**, 4110.
6. Addadi, L., Moradian, J., Shay, E., Maroudas, N. G., Weiner, S. (1987) A chemical model for the cooperation of sulfates and carboxylates in calcite crystal nucleation: Relevance to biomineralization. *Proc. Natl. Acad. Sci.* **84**, 2732-2736.
7. Heywood, B. R., Mann, S. (1994) Template-directed nucleation and growth of inorganic materials. *Adv. Mater.* **6**, 9-20.
8. Berman, A., Ahn, D. J., Lio, A., Salmeron, M., Reichert, A., Charych, D. (1995) Total alignment of calcite at acidic polydiacetylene films: cooperativity at the organic-inorganic interface. *Science* **259**, 515-518.
9. Litvin, A. L., Valiyaveetil, S., Kaplan, D. L., Mann, S. (1997) Template-directed synthesis of aragonite under supramolecular hydrogen-bonded langmuir monolayers. *Adv. Mater.* **9**, 124-127.
10. Aizenberg, J., Black, A. J., Whitesides, G. M. (1999) Control of crystal nucleation by patterned self-assembled monolayers. *Nature* **398**, 495-498.
11. Aizenberg, J. (2004) Crystallization in Patterns: A bio-inspired approach. *Adv. Mater.* **16**, 1295-1302.
12. Pokroy, B., Zolotoyabko, E. (2005) Aragonite growth on single-crystal substrates displaying a threefold axis. *Chem. Comm.* 2140-2142.
13. Gibbs, J. W. (1876) On the equilibrium of heterogeneous substances. *Trans. Connect. Acad. Sci.* **3**, 108-248.
14. Chernov, A. A. (1984). Modern Crystallography III: Crystal Growth. *Springer, Berlin* 978-3-642-81835-6.

15. De Yoreo, J. J., Vekilov, P. G., Dove, P.M., Weiner Eds, S. (2003) Principles of crystal nucleation and growth. In *Biomaterialization* 57-93. *Mineral Soc. Am., Washington, DC* 10.2113/054005.
16. Bernstein, J. (2007) *Polymorphism in Molecular Crystals* (Oxford University Press, Oxford, UK).
17. Lowenstam, H. A., Weiner, S. (1989) *On Biomineralization* (Oxford University Press, Oxford, UK).
18. Mann, S., Ozin, G. A. (1996) Synthesis of inorganic materials with complex form. *Nature* **382**, 313.
19. Dove, P. M., Weiner, S., De Yoreo, J. J. (2003) Biomineralization. *Rev. Mineral. Geochem.* **54**.
20. Mann, S. (2001) *Biomineralization*. (Oxford University Press, Oxford, UK).
21. Sommerdijk, N. A. J. M., De With, G. (2008) Biomimetic CaCO₃ mineralization using designer molecules and interfaces. *Chem. Rev.* **108**, 4499–4550.
22. Kabalah-Amitai, L., Mayzel, B., Kauffmann, Y., Fitch, A. N., Bloch, L., Gilbert, P. U., Pokroy, B. (2013) Vaterite crystals contain two interspersed crystal structures. *Science* **340**, 454-457.
23. Kim, I. W., Robertson, R. E., Zand, R. (2003) Selected polymorphs of CaCO₃ through epitaxy with inorganic substrates aligned with an electric field. *Adv. Mater.* **15**, 709-712.
24. Plummer, L. N., Wigley, T. M. L., Parkhurst, D. L. (1978) The kinetics of calcite dissolution in CO₂ -water systems at 5 degrees to 60 degrees C and 0.0 to 1.0 atm CO₂. *Amer. J. Sci.* **278**, 179-216.
25. Chou, L., Garrels, R. M., Wollast, R. (1989) Comparative study of the kinetics and mechanisms of dissolution of carbonate minerals. *Chem. Geol.* **78**, 269-282.
26. Compton, R. G., Pritchard, K. L. (1990) The dissolution of calcite at pH > 7: kinetics and mechanism. *Phil. Trans. Roy. Soc. London*, **A330**, 47-70.
27. Inskeep, W. P., Bloom, P. R. (1985) An evaluation of rate equations for calcite precipitation kinetics at pCO₂ less than 0.01 atm and pH greater than 8. *Geochimica et Cosmochimica*, **49**, 2165-2180.
28. García-Ruiz, J. M., Amoros, J. L. (1981) Morphological aspects of some symmetrical aggregates grown by silica gel technique. *J. Cryst. Growth* **55**, 379-383.
29. García-Ruiz, J. M. *et al.* (2003) Self-assembled silica-carbonate structures and detection of ancient microfossils. *Science* **302**, 1194-1197.
30. Noorduyn, W. L., Grinthal, A., Mahadevan, L., Aizenberg, J. (2013) Rationally designed complex, hierarchical microarchitectures. *Science* **340**, 832-837.
31. Kaplan, C. N. *et al.* (2017) Controlled growth and form of precipitating microstructures. *Science* **355**, 1395-1398.
32. Gower, L. A., Tirrell, D. A. (1998) Calcium carbonate films and helices grown in solutions of poly(aspartate). *J. Cryst. Growth* **191**, 153-160.
33. Sims, S. D., Didymus, J. M., Mann, S. (1995) Habit modification in synthetic crystals of aragonite and vaterite. *J. Chem. Soc., Chem. Comm.* **10**, 1031-1032.

Figures

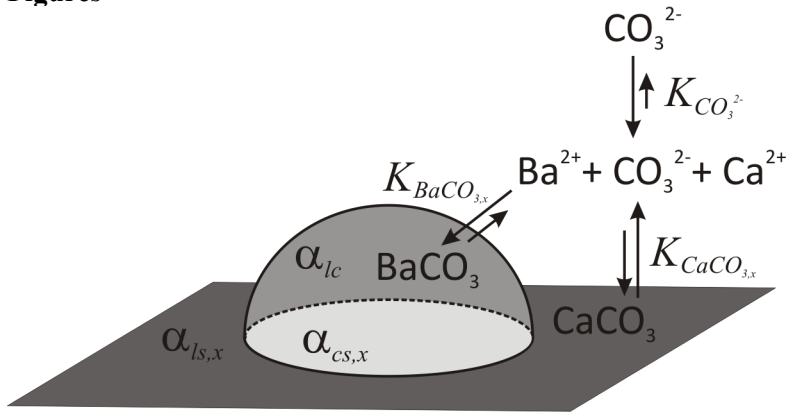


Fig. 1. Nucleation of BaCO_3 on a CaCO_3 substrate. The energy barrier for nucleation is determined by (i) the contributions of the interfacial free energies arising from the lattice mismatch between liquid-crystal α_{lc} , liquid-substrate $\alpha_{ls,x}$ and substrate-crystal $\alpha_{cs,x}$, and (ii) the local supersaturation, which depends on the concentration of ions in the solution, the influx of CO_3^{2-} , the crystallization rate of BaCO_3 and dissolution rate of CaCO_3 , k_{BaCO_3} and $k_{\text{CaCO}_{3,x}}$ respectively for a specific crystal structure x . By controlling the influx of the CO_3^{2-} , the balance can be shifted from the major contribution from the lattice mismatch at high $[\text{CO}_3^{2-}]_{\text{bulk}}$ to a local supersaturation-dominated process controlled by the differences in the solubility of CaCO_3 polymorphs at low $[\text{CO}_3^{2-}]_{\text{bulk}}$. Note that the hemispherical representation is chosen for illustrative purposes and will depend on the specific nucleation conditions.

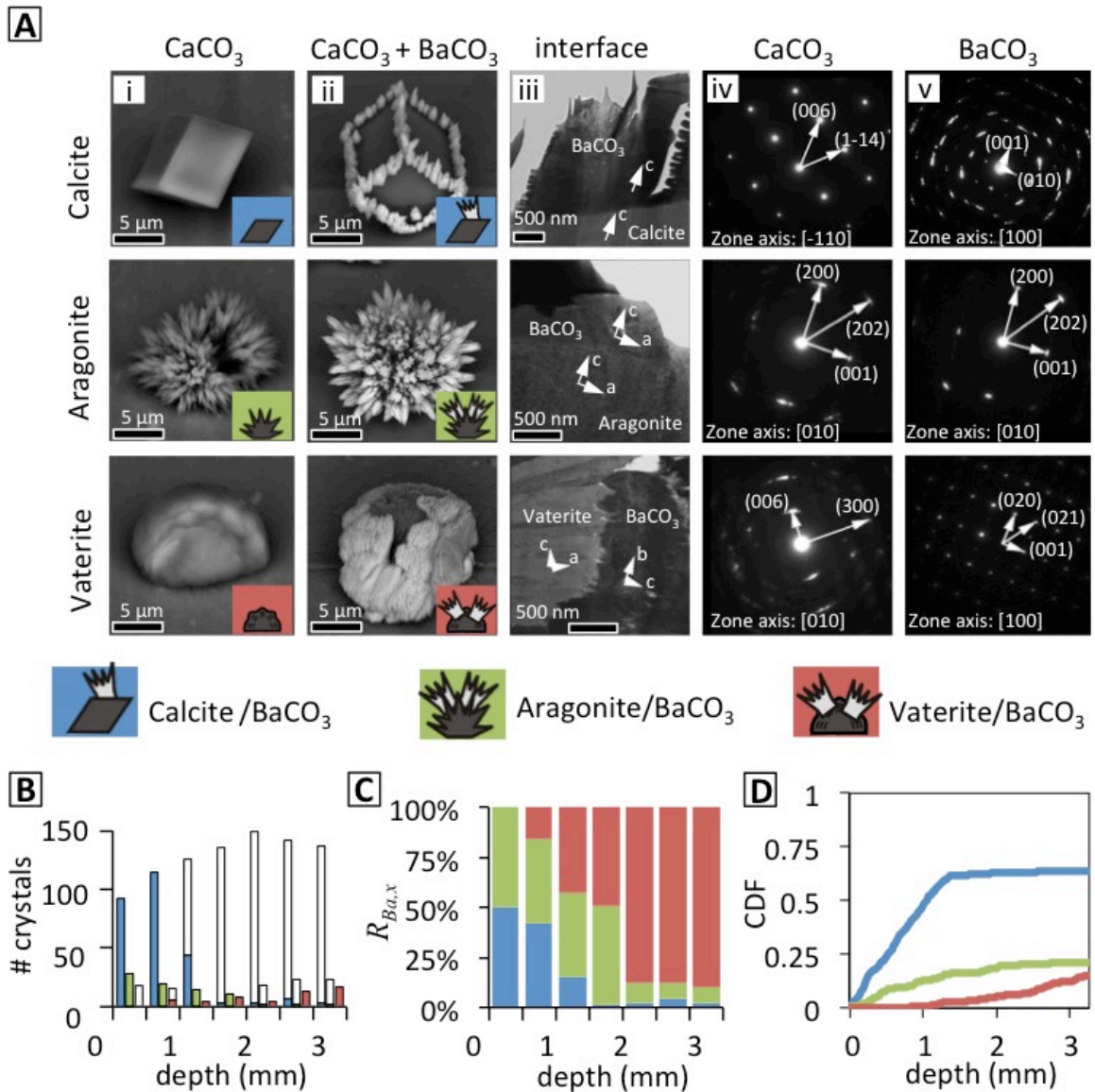


Fig. 2. Polymorph-selective nucleation of BaCO₃ on different CaCO₃ polymorphs. (A) Backscatter electron microscopy images were used to highlight the difference between BaCO₃ (appearing light) on different polymorphs of CaCO₃ (appearing dark). The lattice mismatches were estimated by measuring the crystallographic alignment of BaCO₃ on calcite, aragonite and vaterite (See SI). (ii) BaCO₃ crystals on top of the different polymorphs of CaCO₃. (iii-v) Transmission electron microscopic imaging and corresponding selected area electron diffraction at the interface revealed crystallographic alignment of two axes of BaCO₃ on top of both calcite and aragonite, whereas no crystallographic alignment was found on vaterite. (B-D) Three representations of statistical data of CaCO₃ overgrowth: (B) Total number of various polymorphs of CaCO₃ crystals as a function of depth: calcite (left bar), aragonite (middle bar) and vaterite (right bar). The number of the overgrown CaCO₃ crystals in each category are shown as filled bars: calcite-BaCO₃ (blue), aragonite-BaCO₃ (green) and vaterite-BaCO₃ (red); (C) Polymorph ratio based on data in figure 2B, highlighting that close to the meniscus BaCO₃ nucleation only occurs on calcite and aragonite, and deeper in the solution – only on vaterite; (D) Cumulative distribution function (CDF) of the overgrown crystals as a function of depth.

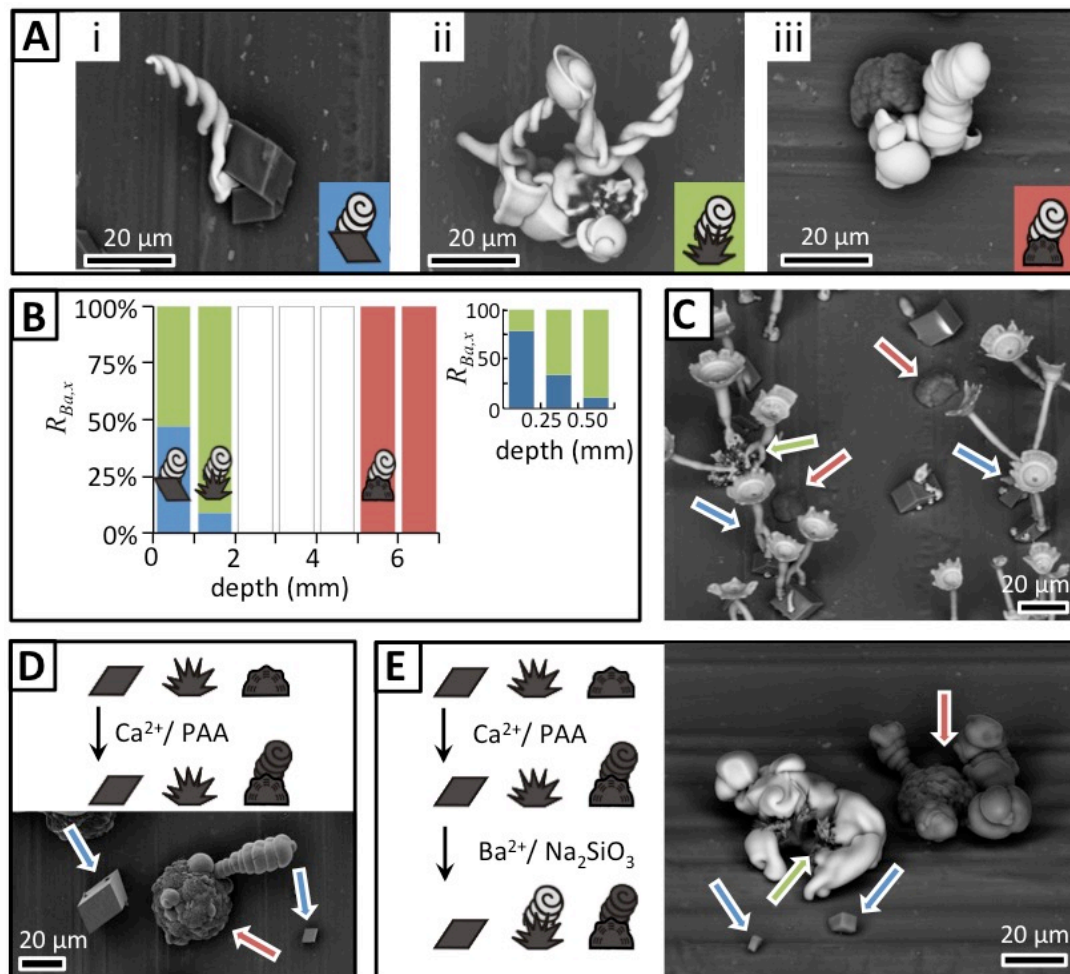


Fig. 3. Polymorph-selective nucleation of $BaCO_3/SiO_2$ and $CaCO_3/PAA$ microstructures. (A) Backscatter scanning electron microscopy images of $BaCO_3/SiO_2$ grown on (i) calcite, (ii) aragonite and (iii) vaterite. (B) Polymorph ratio showing that $BaCO_3/SiO_2$ structures can selectively nucleate on $CaCO_3$ polymorphs by controlling the depth of immersion (see also SI). Inset at top right shows a more detailed polymorph ratio for the depth of 0-0.75 mm. (C) $SrCO_3/SiO_2$ stems that were opened into vases and decorated with serrated edges that selectively nucleated on calcite (blue arrow) and aragonite (green arrow) while vaterite (red arrow) is left empty. (D) $CaCO_3/PAA$ spirals selectively nucleate on vaterite crystals. (E) Sequential nucleation steps can be used to first grow $CaCO_3/PAA$ spirals (dark) on vaterite (dark) and subsequently place $BaCO_3$ spirals (light) on aragonite while leaving calcite empty.

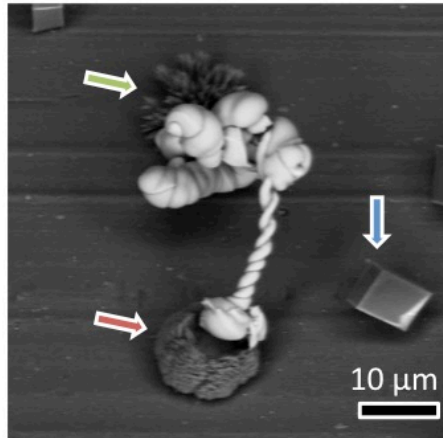
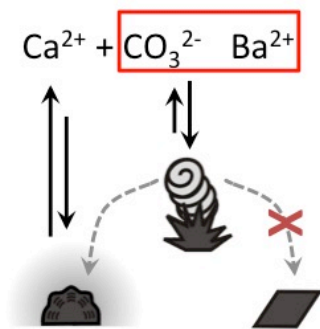


Fig. 4. Polymorph directed nucleation and growth. The balance between the local supersaturation and lattice mismatch can be controlled by the influx of CO_2 such that nucleation of a $\text{BaCO}_3/\text{SiO}_2$ microstructure first occurs at aragonite (green arrow) and subsequently grows towards nearby dissolving vaterite (red arrow) while leaving nearby calcite unaffected (blue arrow). The dotted arrow represents the direction of growth.